WWW.IJRPR.COM

International Journal of Research Publication and Reviews

Journal homepage: www.ijrpr.com ISSN 2582-7421

To Study the Impacts of Chemical Reaction and Thermal Radiations on the Flow of Casson Nanofluid

Muhammad Awais[1], Muhammad Amad Sarwar[2*], Muhammad Mukhtar Khan[3], Jawad Hasanain[4]

[1] Department of Mathematics, University of Sialkot, Sialkot, Punjab province, Pakistan. (awaissahi9137@gmail.com)

[2*]School of Mathematics, Nanjing University of Aeronautics and Astronautics, Nanjing, Jiangsu province, 211106, PR China. (m.amadsarwar26@gmail.com)

[3, 4] Department of Mathematics, international Islamic university islamabad, Pakistan

ABSTRACT:

This study delves into optimizing heat transfer by integrating nanoparticles into working fluids, forming nanofluids. Examining applications across diverse fields, it investigates micropolar fluid flow, partial slip effects, MHD-influenced viscous fluid flow, and calorific properties of nanofluids. Utilizing the Casson model, the research explores nanofluid flow with thermal radiation entropy generation, extending to porous surfaces and Lorentz force effects. It also addresses viscoelastic fluid models and catalytic reactions in porous media, studying reactions across oscillating discs, nanofluid flows with autocatalytic processes, and electromagnetic effects in ferromagnetic Jeffrey nanofluids. Additionally, the study explores the catalytic role of porous media in chemical reactions, varying disc thicknesses, and heat application of Al_2O_3 nanoparticles in microchannels. This comprehensive overview contributes to understanding nanofluids' diverse applications, encapsulating various influential factors within a limited word count, fostering advancements in thermal productivity and resource management.

1. Introduction:

One major problem with several heat transfer components when designing applications is the low thermal efficiency of the working fluid. In order to establish a creative strategy for increasing the thermal productivity of working liquids, certain scientists are currently preoccupied with this issue. To increase the thermal productivity of liquids, a variety of components have been suggested by experts. Therefore, the employment of nanoparticles in working liquids, also known as nanofluids, is an especially alluring element. Working fluid offers a number of benefits when nanoparticles are integrated, according to recent studies on the subject. This is due to the fact that working fluids' thermal productivity is lower than that of nanofluids. A type of liquids known as nanofluids, which contain functioning liquid with nanoscale particles, has only lately come into existence. These nanoparticles are used in a variety of devices, including MHD control generators, oil reservoirs, atomic reactor cooling, cancer treatment, automobile transformers, and more by researchers via [2-6]. Khan et al. [7] studies the use of modified thermodiffusion expressions for the flow of micropolar fluid with a time-dependent thermal process. Mustafa et al. [8] investigations into the impact of a revolving disk partial slip state on the investigation of nanofluid flow. Hafeez et al. [9] studied how the flow of viscous fluids is impacted by MHD and the entropy produced by rotating disk. Baleanu et al. [10] have calculated the gender of nanofluids' calorific ownership. More contributions from the flow of nanofluids can be found in the references [11-15]. Song et al. [16] investigated the heat and mass parameters of a third-grade nanofluid in the presence of a fluctuating reactive index.

The Casson model is one of the non-Newtonian models that is crucial for understanding the complex rheological behaviours of biological fluids. By using two stretching discs, Siddiqui et al. [17] evaluated the impact of thermal radiation entropy generation on the Casson nanofluid flow. The study for viscoelastic fluids should be modified To generalise the behaviour of viscoelastic fluid models, the Casson liquid model is presented. It follows from the literature that the Casson model, which achieves yield stress, is the most appropriate model for describing the rheological behaviour of viscoelastic flows. The effects of radiation and Casson fluid flow on a porous exponential stretching surface were investigated by Khan et al. [18]. Shaheen et al. [19] have quantitatively studied the effects of the Lorentz force on a nonlinear radiative Casson fluid flow containing gold nanoparticles. Jyothi et al. [20] elaborated the blood flow through a Casson liquid and a stretched geometry using magnetohydrodynamics.

The homogeneous-heterogeneous reaction only occurs when a catalyst is present. A catalyst increases the rate at which the chemical reaction proceeds. But when surface catalysed chemical reactions occur, the rate of reaction is accelerated. Yu et al.[21] investigated porous media when investigating the effect of the surface catalysed parameter. Hayat et al. [22] studies the movement of chemically reactive nanomaterials across an oscillating disc of different thicknesses. Mehmood et al. [23] analyse two distinct nanofluid flow combinations, namely copper-water and alumina-water, across a spinning disc to see how autocatalytic chemical processes and melting heat transfer affect the flow. Song et al. [24] provided the electromagnetic dipole and gyrotactic microorganisms in the ferromagnetic Jeffrey nanofluid were examined using thermal radiative analysis. Khan et al. [25] directed the heat application of Al_2O_3 nanoparticles suspended in water and contained by a microchannel.

2. Problem Formulation:

The study will be conducted using the (r, ϕ, z) cylindrical coordinate system. Imagine a nanofluid flowing across an infinite, flat disc that is located in the plane $z = 0$. The half-space $z > 0$ contains a nanofluid that conducts electricity and is not compressible. The disc rotates in the positive ϕ direction at a fixed angular velocity λ, which results in flow. Partial slip conditions are believed to be applicable since the boundary layer thickness is expected to be less than the typical scale of roughness at the disk. The axial direction is followed by a magnetic field with constant intensity B_0. According to this hypothesis, the induced magnetic field is negligible because to the low magnetic Reynolds number. T_w and T_∞ are used to represent the wall and ambient temperature, respectively, where T_w is greater than T_∞. The axial symmetry of the issue prevents the inclusion of the derivatives with respect to the coordinates ϕ.

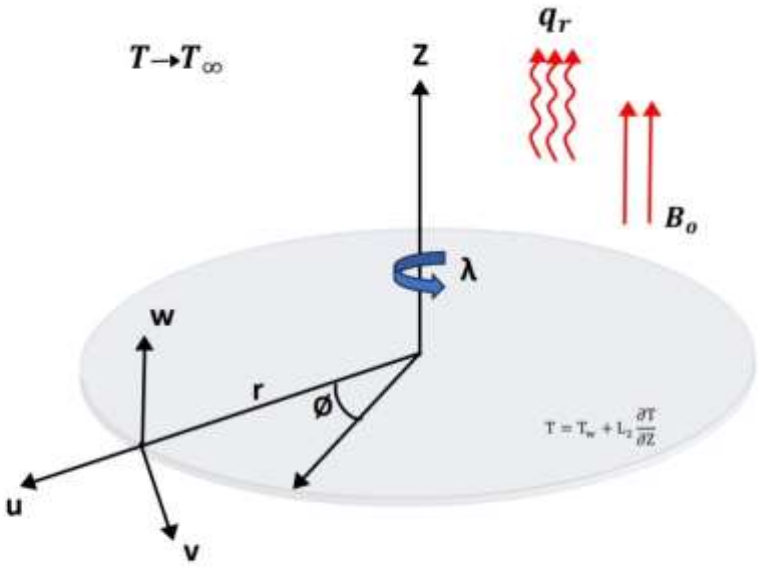

Figure 1. Problem geometry and the coordinate system.

The following are the present flow's governing equations:

$$\frac{\partial u}{\partial r} + \frac{u}{r} + \frac{\partial w}{\partial z} \quad (1)$$

$$\left(u\frac{\partial u}{\partial r} - \frac{v^2}{r} + w\frac{\partial u}{\partial z}\right) = \nu\left(1 + \frac{1}{\beta}\right)\left(\frac{\partial^2 u}{\partial r^2} + \frac{1}{r}\frac{\partial u}{\partial r} - \frac{u}{r^2} + \frac{\partial^2 u}{\partial z^2}\right) - \frac{\sigma B_0^2 u}{\rho} \quad (2)$$

$$\left(u\frac{\partial v}{\partial r} - \frac{uv}{r} + w\frac{\partial v}{\partial z}\right) = \nu\left(1 + \frac{1}{\beta}\right)\left(\frac{\partial^2 v}{\partial r^2} + \frac{1}{r}\frac{\partial v}{\partial r} - \frac{v}{r^2} + \frac{\partial^2 v}{\partial z^2}\right) - \frac{\sigma B_0^2 v}{\rho} \quad (3)$$

$$\left(u\frac{\partial w}{\partial r} + w\frac{\partial w}{\partial z}\right) = \nu\left(1 + \frac{1}{\beta}\right)\left(\frac{\partial^2 w}{\partial r^2} + \frac{1}{r}\frac{\partial w}{\partial r} + \frac{\partial^2 w}{\partial z^2}\right) \quad (4)$$

$$u\frac{\partial T}{\partial r} + w\frac{\partial T}{\partial z} = \alpha_f\left(\frac{\partial^2 T}{\partial r^2} + \frac{1}{r}\frac{\partial T}{\partial r} + \frac{\partial^2 T}{\partial z^2}\right) + \tau\left[D_B\left(\frac{\partial T}{\partial r}\frac{\partial C}{\partial r} + \frac{\partial T}{\partial z}\frac{\partial C}{\partial z}\right) + \frac{D_T}{T_\infty}\left\{\left(\frac{\partial T}{\partial r}\right)^2 + \left(\frac{\partial T}{\partial z}\right)^2\right\}\right] - \frac{\partial q_r}{\partial z} \quad (5)$$

$$u\frac{\partial C}{\partial r} + w\frac{\partial C}{\partial z} = D_B\left(\frac{\partial^2 C}{\partial r^2} + \frac{1}{r}\frac{\partial C}{\partial r} + \frac{\partial^2 C}{\partial z^2}\right) + \frac{D_T}{T_\infty}\left(\frac{\partial^2 T}{\partial r^2} + \frac{1}{r}\frac{\partial T}{\partial r} + \frac{\partial^2 T}{\partial z^2}\right) - R^*(C - C_\infty) \quad (6)$$

Where u, v, and w represent the velocity components in the directions of increasing $r, \phi, and\ z$, T stands for local fluid temperature, the letters C stand for nanoparticle concentration, P stands for pressure, β stands for Casson fluid parameter, α_f stands for the thermal diffusivity of a nanofluid, the coefficient of thermophoretic diffusion is D_T and τ is the ratio of the heat capacity of the base liquid to the substance containing the nanoparticles.

The following conditions apply to the problem:

$$u = L_1\frac{\partial u}{\partial z}, v = r\lambda + L_1\frac{\partial v}{\partial z}, w = 0, T = T_w + L_2\frac{\partial T}{\partial z}, C = C_w + L_3\frac{\partial C}{\partial z}\ at\ z = 0$$

$$u \to 0, v \to 0, T \to T_\infty, C \to C_\infty,\ as\ z \to \infty \quad (7)$$

Where the nanofluid's temperature is T, T_∞ is the ambient nanofluid's temperature, p stands for pressure, the pressure of the ambient nanofluid is p_∞.

$$\eta = \sqrt{\frac{2\lambda}{\nu_f}}\, z, \quad u = r\lambda f'(\eta),\ v = r\lambda g(\eta),\ w = -\sqrt{2\nu_f\lambda}\, f(\eta),$$

$$T = T_\infty + (T_w - T_\infty)\theta(\eta),\ C = C_\infty + C_\infty\phi(\eta), \quad (8)$$

The non-dimensional distance along the rotational axis is denoted by η, whereas $f, g, \theta \; and \; \phi$ represent non-dimensional functions of η. Equation (3.1) is already satisfied by transformation (3.8), while equations (3.2), (3.3), (3.5) and (3.6) assume the following forms:

$$\left(1+\frac{1}{\beta}\right) f''' + ff'' - \frac{1}{2}f'^2 + \frac{1}{2}g^2 - Mf' = 0, \quad (9)$$

$$\left(1+\frac{1}{\beta}\right) g'' + fg' - f'g - Mg = 0, \quad (10)$$

$$\frac{1}{Pr}\left(1+\frac{4N}{3}\right)\theta'' + f\theta' + Nb\theta'\Phi' + Nt\theta'^2 = 0 \quad (11)$$

$$\Phi'' + Sc\, f\Phi' + \frac{Nt}{Nb}\theta'' - Sc\, R\, \Phi = 0 \quad (12)$$

The boundary conditions of equation (7) become

$$f(0) = 0,\ f'(0) = \alpha f''(0),\ \mathrm{g}(0) = 1 + \alpha g'(0),\ \theta(0) = 1 + \beta\theta'(0),\ \phi(0) = 1 + \gamma\phi'(0) \text{ at } \eta = 0$$

$$f' \to 0, \mathrm{g} \to 0, \theta \to 0, \phi \to 0 \text{ at } \eta \to \infty \quad (13)$$

Where the word prime denotes a derivative with respect to η, a magnetic field is represented by M, Prandtl number is Pr, the Schmidt number is denoted by Sc, the parameter for Brownian motion is Nb, Nt the thermophoresis parameter.

These are described below:

$$M = \frac{\sigma B_0^2}{2\rho\lambda}, Pr = \frac{\nu_f}{\alpha_f},\ Sc = \frac{\nu_f}{D_B}, Nb = \frac{\tau D_B C_\infty}{\nu_f}, Nt = \frac{\tau D_T (T_w - T_\infty)}{T_\infty \nu_f}, Nt_b = \frac{Nt}{Nb}. \quad (14)$$

To quickly determine a nanofluid's pressure, observe that equation (4) can be integrated. The resistive torque on the disc with radius R in this instance, as given by the definite integral, is the quantity of practical interest. Additionally, the tangential stress τ_θ and radial stress τ_r are determined as follows:

$$\tau_r = \mu\left(\frac{\partial u}{\partial r} + \frac{\partial w}{\partial r}\right)_{z=0} = \mu r\lambda\sqrt{\frac{2\lambda}{\nu_f}}\, f''(0),$$

$$\tau_\theta = \mu\left(\frac{\partial v}{\partial z}\right)_{z=0} = \mu r\lambda\sqrt{\frac{2\lambda}{\nu_f}}\, g'(0), \quad (15)$$

and the skin friction coefficient that follows

$$C_f = \frac{\sqrt{\tau_r^2 + \tau_\theta^2}}{\rho(r\lambda)^2} = \sqrt{\frac{2\nu}{r^2\lambda}}\,(f''(0)^2 + g''(0)^2)^{\frac{1}{2}}. \quad (16)$$

The local Nusselt number Nu_r is determined by calculating the heat flow as the sum of the conduction heat flux (fourier-law) and the heat flux arising from nanoparticle diffusion.

$$Nu_r = -\frac{\left(\frac{\partial T}{\partial z}\right)_{z=0}}{(T_w - T_\infty)} = -\sqrt{\frac{2\lambda}{\nu_f}}\,\theta'(0) = -\sqrt{\frac{2\lambda}{\nu_f}}\,\theta'(0). \quad (17)$$

3. Result and discussion

The Keller-box Method, a finite difference scheme, is used to numerically solve the coupled nonlinear ordinary differential equations (9–12) subjected to the boundary conditions (13). Numerical outcomes for physical parameters of interest like as M represents a magnetic field, the Prandtl number is Pr, the Schmidt number is denoted by Sc, the parameter for Brownian motion is Nb, Nt the thermophoresis parameter, N is the parameter of thermal radiation and R is the parameter of chemical reaction. Table 1 describes a comparison of f', f'', and g' by fixing the parameters M, γ. Table 2 $\theta'(0)$ data are expressed numerically and represent the rate of heat transfer at the disk. The thermophoresis parameter Nt is increased, which results in an increase in $\theta'(0)$ magnitude. Physically, as the thermophoretic effect becomes stronger, highly thermally conductive nanoparticles go deeper into the fluid, thickening the thermal boundary layer. As a result, thicker temperature profiles are responsible for the observed decreasing wall temperature gradient. When the thermal slip coefficient increases, the local Nusselt number also decreases. On the other hand, the Prandtl number contrasts the momentum and heat diffusion coefficients. Thermal diffusivity is known to affect thermal boundary layer thickness. Greater Prandtl number Pr denotes less thermal diffusivity, which results in a thinner thermal boundary layer and slower growth of the boundary layer thickness than for smaller Prandtl number fluids. Larger temperature slope near the wall compensates for a thinner thermal boundary layer.

Table 1. Contrast of $f''(0)$ and $g'(0)$ for different values of M and γ for λ_1=0 and R=0 when β→∞

M	α	Mustafa (2017) $f'(0)$	Mustafa (2017) $f''(0)$	Mustafa (2017) $g'(0)$	Present Results $f'(0)$	Present Results $f''(0)$	Present Results $g'(0)$
0	0.25	0.064883	0.259534	-0.416784	0.064883	0.259534	-0.416784
0.2	0.25	0.047794	0.191176	-0.509536	0.047794	0.191176	-0.509536
0.4	0.25	0.036514	0.146057	-0.599523	0.036514	0.146057	-0.599523
0.6	0.25	0.029175	0.116699	-0.680355	0.029175	0.116699	-0.680355

0.8	0.25	0.024192	0.096762	-0.751543	0.024192	0.096762	-0.751543
0.5	0	0	0.218678	-0.755935	0	0.218678	-0.755935
0.5	0.2	0.028608	0.143038	-0.662149	0.028608	0.143038	-0.662149
0.5	0.4	0.039658	0.099146	-0.584589	0.039658	0.099146	-0.584589
0.5	0.6	0.043151	0.071917	-0.522031	0.043151	0.071917	-0.522031

Table 2. Variations of the $-\theta'(0)$(Nusselt number) for various values of Nb, Nt, Pr, Sc, M, α, β, γ.

Nb	**Nt**	**Pr**	**Sc**	**M**	**R**	**N**	α	β	γ	$-\theta'(0)$
0.1	0.1	6.5	5.0	0.1	1.0	1.0	0.1	0.1	0.5	0.8984
0.3	0.1	6.5	5.0	0.1	1.0	1.0	0.1	0.1	0.5	0.6010
0.1	**0.3**	6.5	5.0	0.1	1.0	1.0	0.1	0.1	0.5	0.7167
0.1	0.1	**10.0**	5.0	0.1	1.0	1.0	0.1	0.1	0.5	0.9902
0.1	0.1	6.5	**10.0**	0.1	1.0	1.0	0.1	0.1	0.5	0.8701
0.1	0.1	6.5	5.0	**0.5**	1.0	1.0	0.1	0.1	0.5	0.8943
0.1	0.1	6.5	5.0	0.1	**3.0**	1.0	0.1	0.1	0.5	0.9188
0.1	0.1	6.5	5.0	0.1	1.0	**3.0**	0.1	0.1	0.5	0.6908
0.1	0.1	6.5	5.0	0.1	1.0	1.0	**0.5**	0.1	0.5	0.9030
0.1	0.1	6.5	5.0	0.1	1.0	1.0	0.1	**1.0**	0.5	0.9051
0.1	0.1	6.5	5.0	0.1	1.0	1.0	0.1	0.1	**1.5**	1.0615

Figure (1) explains how M affects the velocity profile. By improving M, $f'(\eta)$ first increases. It is based on the fact that radial velocity is decreased by Lorentz force which is produced by magnetic field. Figure (2) shows how the thermal slip parameter α change in relation to variations in the velocity profile. As the parameter α enlarge, $f'(\eta)$ decreases. The azimuthal velocity decrease as the value of parameter M is increased. Lorentz force which is produced by field opposes fluid motion in figure (3). Figure (4) describes variations in θ(η) as Pr parameter increases. The proportion of momentum to thermal diffusivity is known as the Prandtl number. θ(η) decreases as this ratio increases. Figure (5) depicts variations in θ(η) as Nt increases. Nt denotes the ratio of momentum diffusion in nanofluids to the rate of nanoparticle diffusion caused by thermophoretic force. As Nt enlarges θ(η) also increase. Figure (6) explains the effect of the Brownian motion parameter (Nb) on the temperature profile θ(η). The temperature profile rises as the Brownian motion parameter's value increases. Figure (7) illustrates that as the value of γ roses from 0.1 to 0.17, there is decrease on temperature profile. The influence of the thermophoresis parameter (Nt) on the concentration profile ϕ(η) is shown in Figure (8). The concentration profile ϕ(η) is expanded with an increase in Nt. Brownian motion parameter (Nb) fluctuations are shown in Figure (9) as a concentration profile ϕ (η). A decrease in ϕ(η) is observed as Nb is increased from 0.1 to 0.5. Figure (10) illustrates the variation in Lewis number (Le) on concentration profile. As Lewis number is increased from 1.0 to 2.5, a decrease in concentration profile is depicted. Figure (11) shows a direct relationship (correspondence) between the concentration profile and the chemical processes R. The concentration profile shows a drop as R is decreased. Due to the use of chemicals during the flow, this happens. Figure (12) demonstrates the impact of radiation on θ(η). Growing N raises the temperature profile. By increasing, the fluid's velocity is raised, which raises the temperature of the thermal boundary layer and generates heat in the flow area.

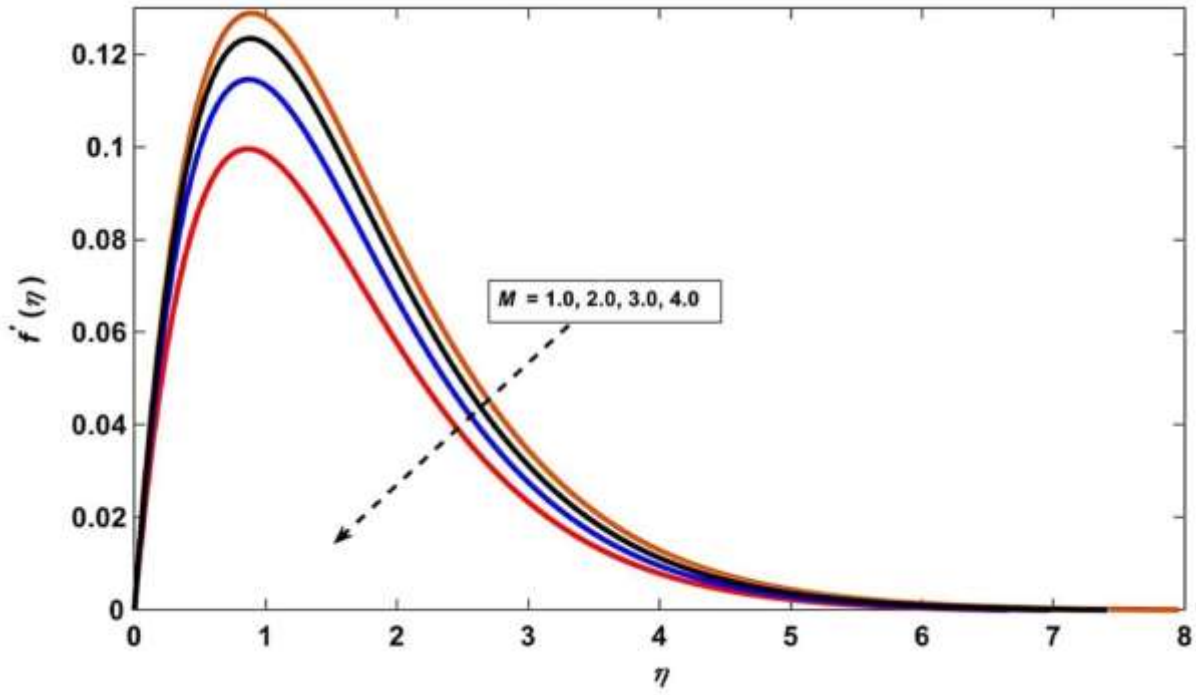

Figure 1. Velocity profile variations for various M values.

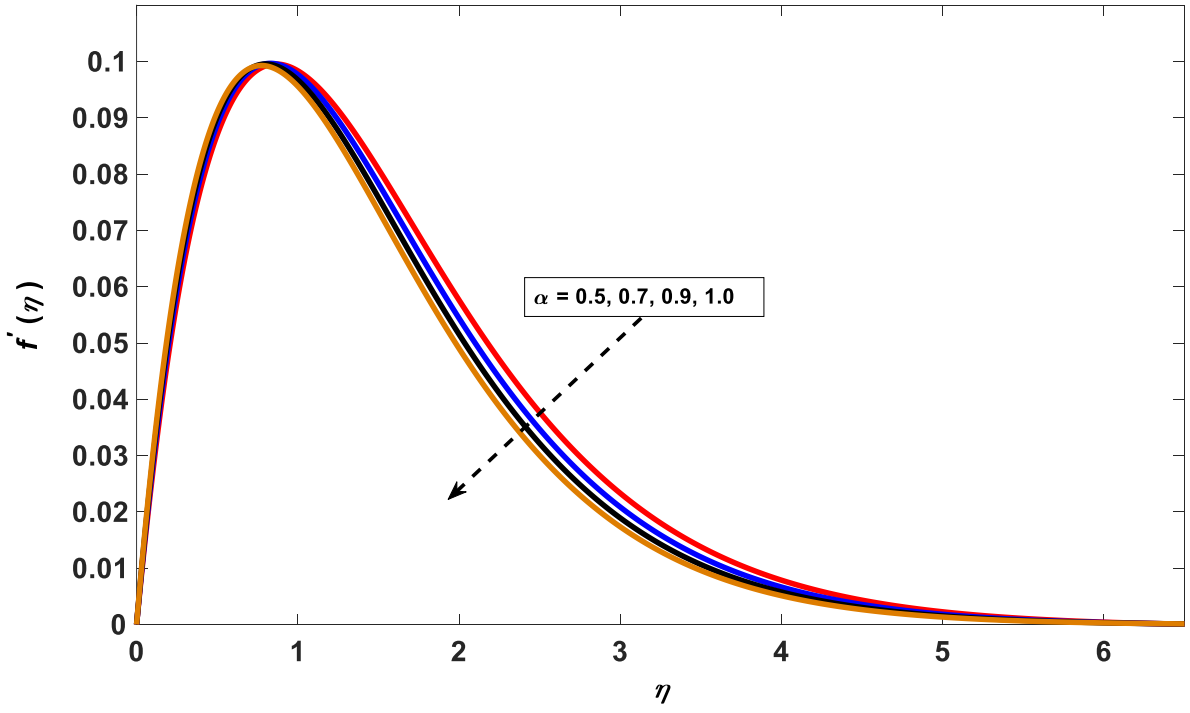

Figure 2. Velocity profile variations for various values of thermal slip coefficient(α).

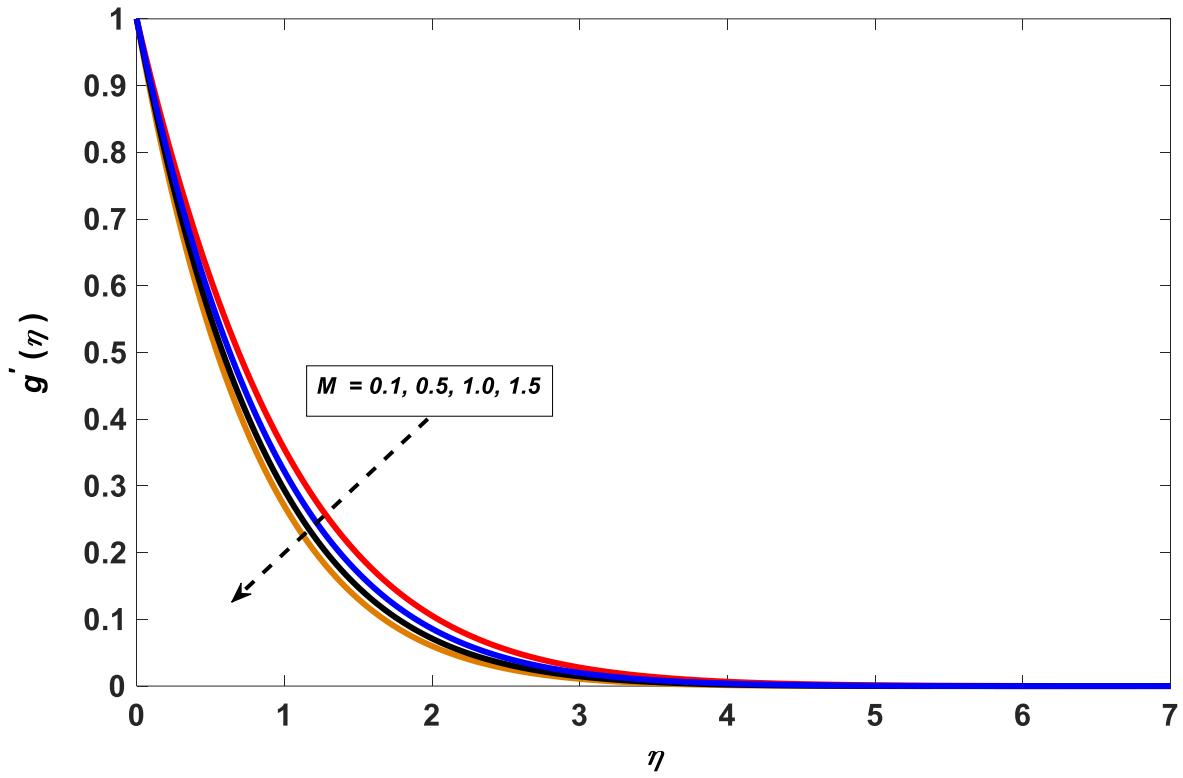

Figure 3. Impact of magnetic field parameter M on azimuthal velocity.

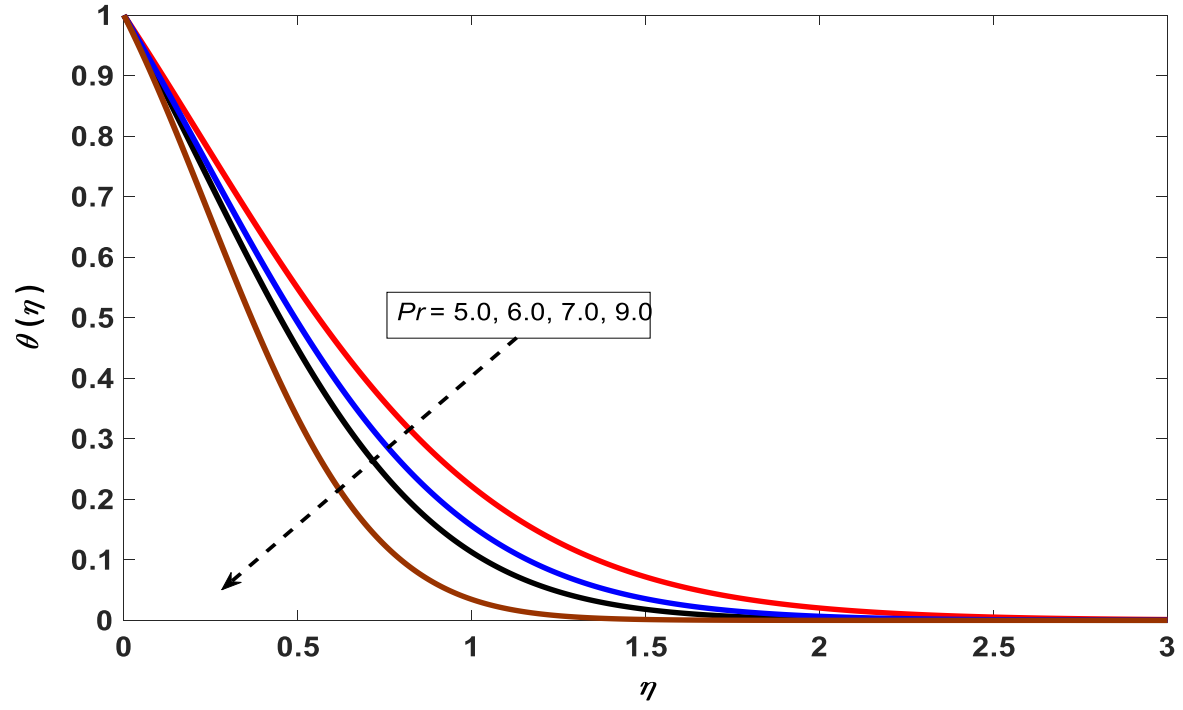

Figure 4. Variation in dimensionless temperature(θ) for various values of prandtl number(Pr).

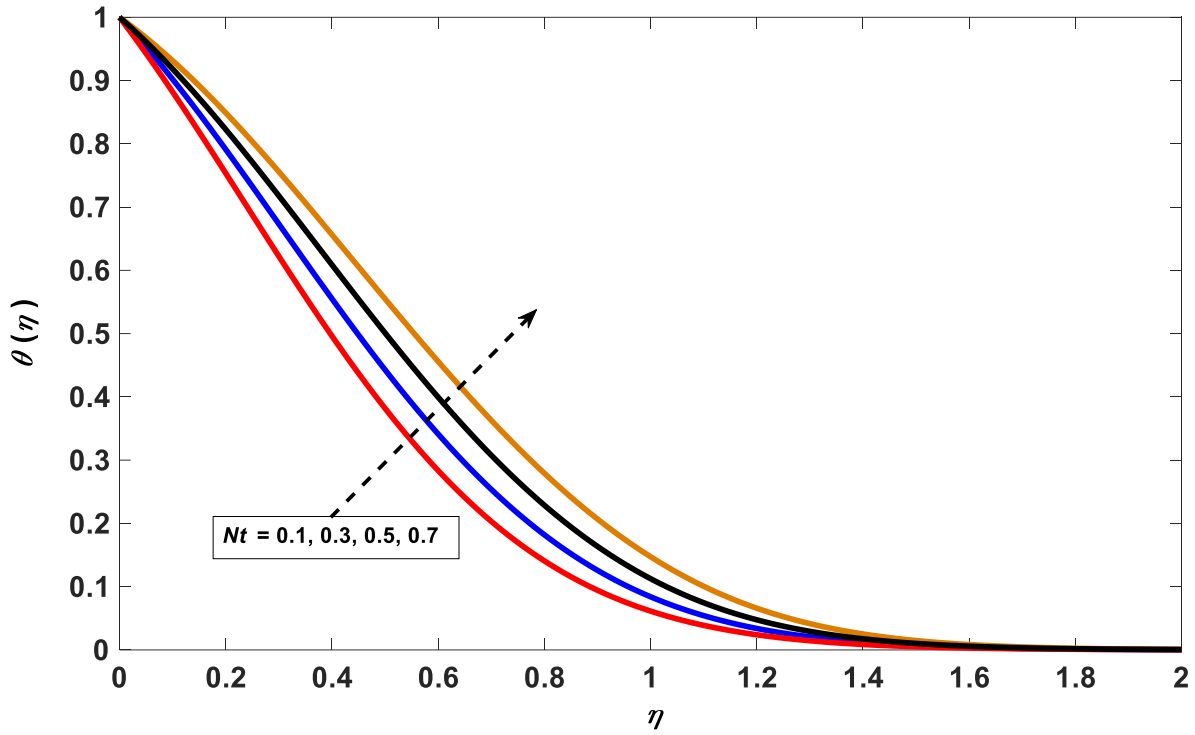

Figure 5. Impact of thermophoresis parameter(Nt) on temperature profile θ(η).

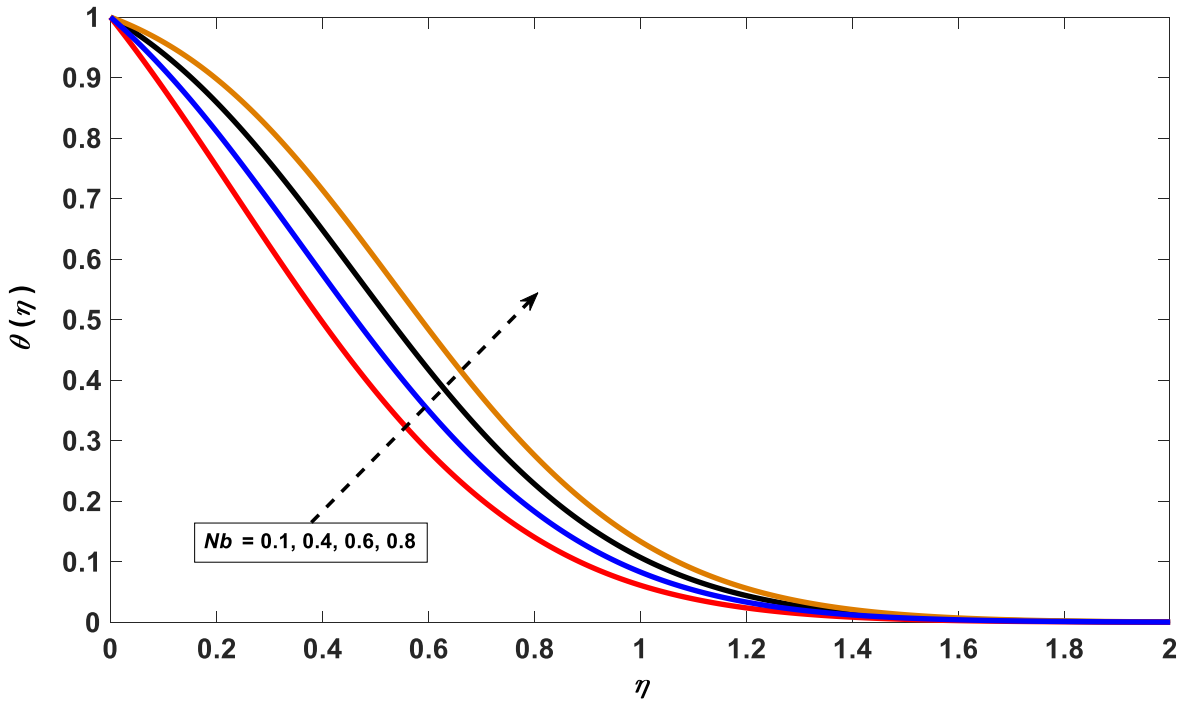

Figure 6. Variety in temperature profile θ(η) for Brownian motion parameter(Nb).

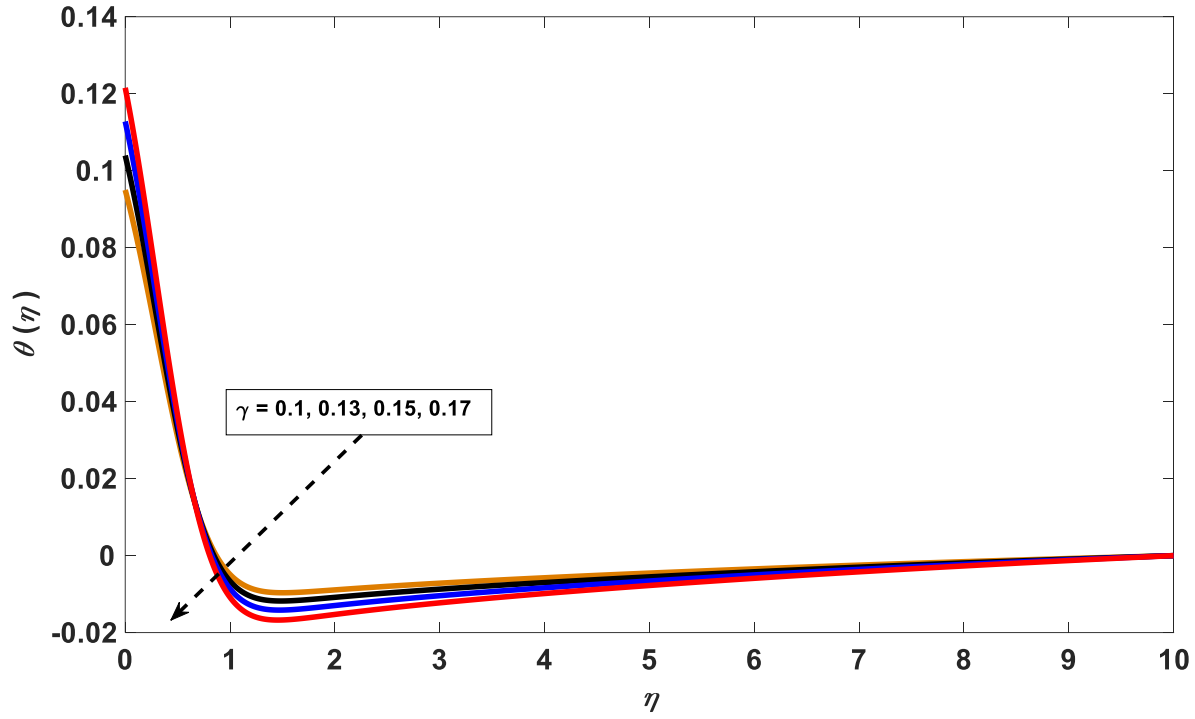

Figure 7. Variation in temperature profile θ(η) for dimensionless velocity slip coefficient (γ).

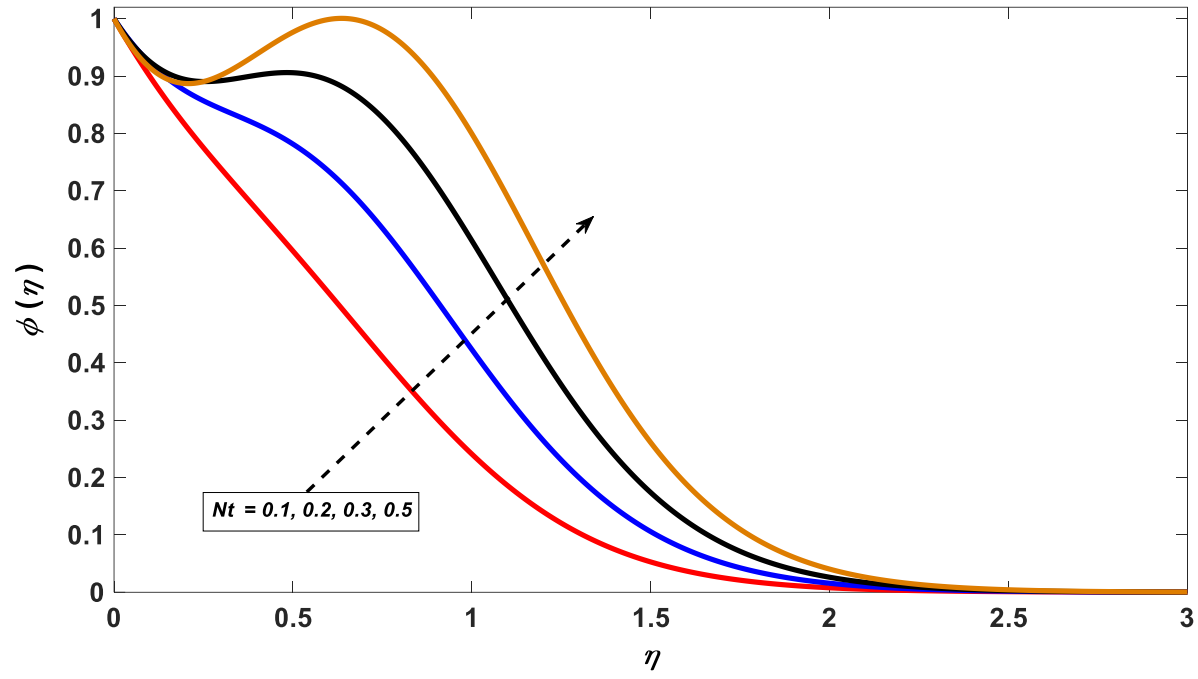

Figure 8. Impact of thermophoresis parameter(Nt) on concentration profile(η).

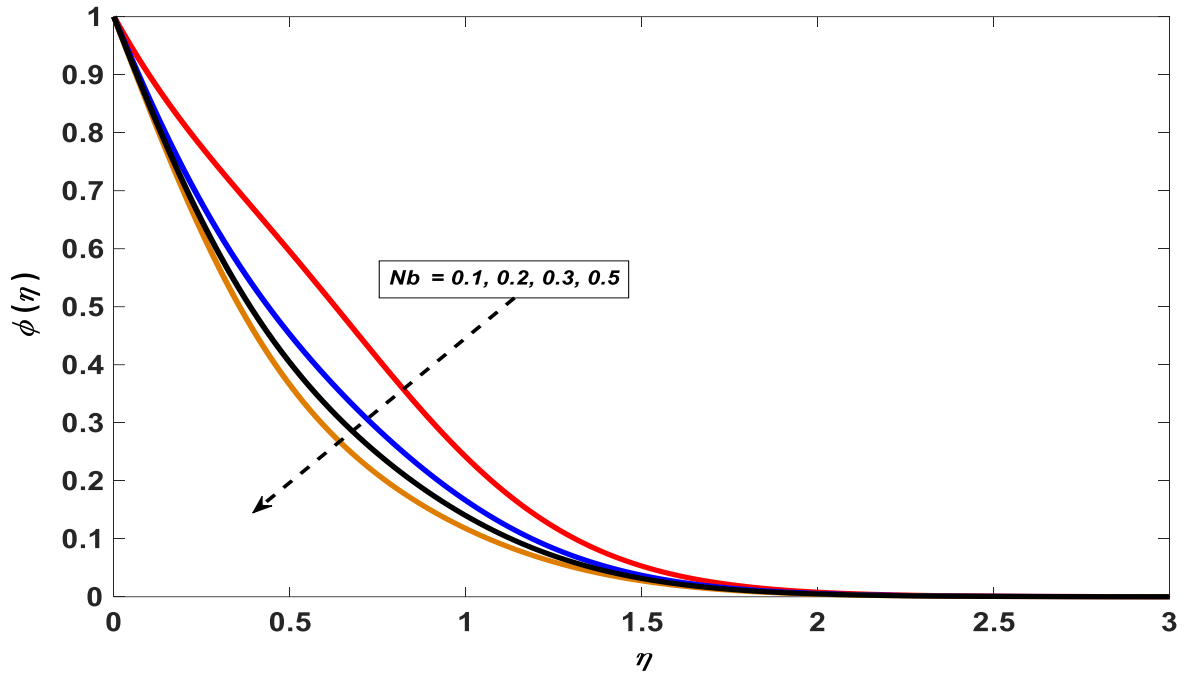

Figure 9. Impact of Brownian motion parameter(Nb) on concentration profile.

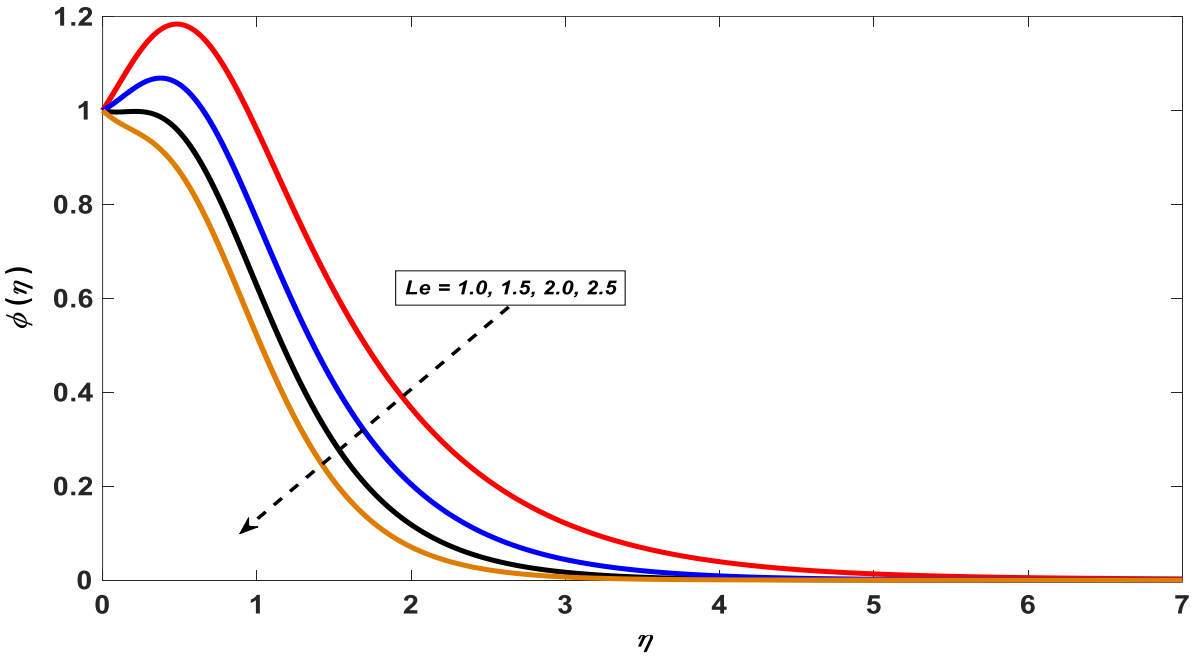

Figure 10. Variety in concentration profile ϕ (η) with variation in Lewis Number(Le).

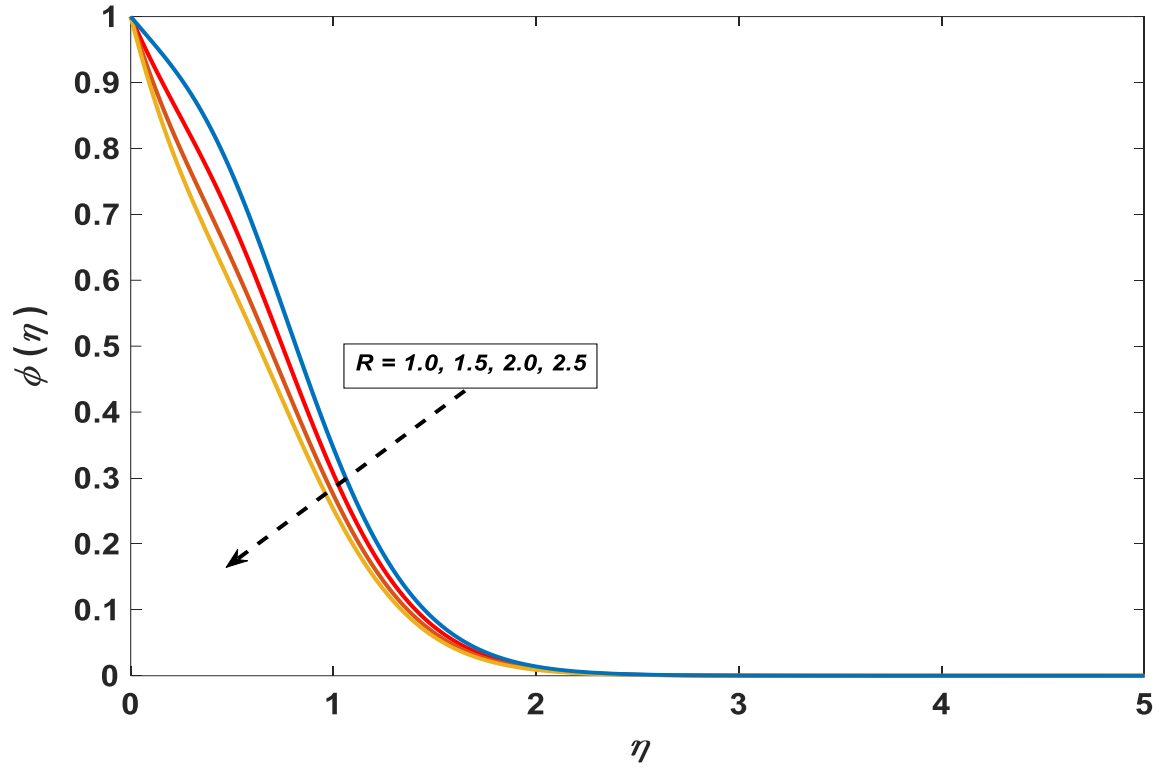

Figure 11. Concentration profile variation for various R values.

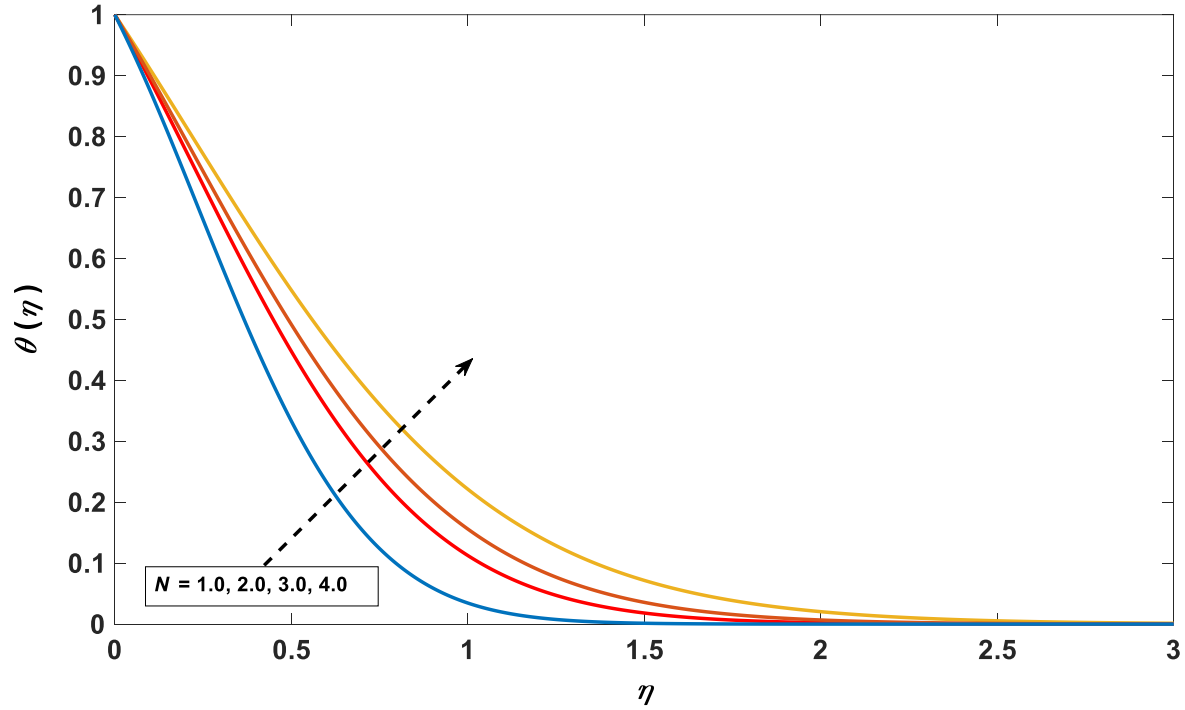

Figure 12. Temperature profile variations for various N values.

4. CONCLUSION

This part of the research investigates numerically the Casson nanofluid flow over rotating disk with chemical reactions. The obtained mathematical model contains the nonlinear PDEs of continuity equation, momentum, heat and mass equations. By using the similarity transformations, these PDEs are additionally transformed into a system of nonlinear ODEs. Brownian motion and features of thermophoresis are included using the Buongiorno model. The Keller Box method is used to numerically solve the governing partial differential equations. The graphical and tabulated data are used to analysis each problem.

i. With the growth of the chemical reaction, $-\theta'(0)$ decreases and $-\phi'(0)$ increases.

ii. The value of the chemical reaction parameter and the thermophoresis parameter both rises, which increases the Nusselt number.

iii. $-\theta'(0)$ reduces and $-\phi'(0)$ rises due to the thermal radiation parameters.

iv. Nusselt number decreases due to increasing the value of radiation parameter and Schmidt number.

References

1. Asma, M., Othman, W. A. M., Muhammad, T., Mallawi, F., & Wong, B. R. (2019). Numerical study for magnetohydrodynamic flow of nanofluid due to a rotating disk with binary chemical reaction and Arrhenius activation energy. Symmetry, 11(10), 1282.
2. Hsiao, K. L. (2014). Nanofluid flow with multimedia physical features for conjugate mixed convection and radiation. Computers & Fluids, 104, 1-8.
3. Wen, B., Corson, L. T., & Chini, G. P. (2015). Structure and stability of steady porous medium convection at large Rayleigh number. Journal of Fluid Mechanics, 772, 197-224.
4. Hsiao, K. L. (2016). Stagnation electrical MHD nanofluid mixed convection with slip boundary on a stretching sheet. Applied Thermal Engineering, 98, 850-861.
5. Hsiao, K. L. (2017). Micropolar nanofluid flow with MHD and viscous dissipation effects towards a stretching sheet with multimedia feature. International Journal of Heat and Mass Transfer, 112, 983-990.
6. Wen, B., Chang, K. W., & Hesse, M. A. (2018). Rayleigh-Darcy convection with hydrodynamic dispersion. Physical Review Fluids, 3(12), 123801.
7. Khan, M. I., Waqas, H., Khan, S. U., Imran, M., Chu, Y. M., Abbasi, A., & Kadry, S. (2021). Slip flow of micropolar nanofluid over a porous rotating disk with motile microorganisms, nonlinear thermal radiation and activation energy. International Communications in Heat and Mass Transfer, 122, 105161.
8. Mustafa, M. (2017). MHD nanofluid flow over a rotating disk with partial slip effects: Buongiorno model. International Journal of Heat and Mass Transfer, 108, 1910-1916.
9. Hafeez, A., Khan, M., & Ahmed, J. (2020). Flow of magnetized Oldroyd-B nanofluid over a rotating disk. Applied Nanoscience, 10, 5135-5147.
10. Baleanu, D., Sadat, R., & Ali, M. R. (2020). The method of lines for solution of the carbon nanotubes engine oil nanofluid over an unsteady rotating disk. The European Physical Journal Plus, 135, 1-13.
11. Ramesh, G. K., Roopa, G. S., Shehzad, S., & Khan, S. U. (2020). Interaction of Al2O3-Ag and Al2O3-Cu hybrid nanoparticles with water on convectively heated moving material. Multidiscipline Modeling in Materials and Structures, 16(6), 1651-1667.
12. Khan, S. U., Waqas, H., Shehzad, S. A., & Imran, M. (2019). Theoretical analysis of tangent hyperbolic nanoparticles with combined electrical MHD, activation energy and Wu's slip features: a mathematical model. Physica Scripta, 94(12), 125211.
13. Muhammad, T., Waqas, H., Khan, S. A., Ellahi, R., & Sait, S. M. (2021). Significance of nonlinear thermal radiation in 3D Eyring–Powell nanofluid flow with Arrhenius activation energy. Journal of Thermal Analysis and Calorimetry, 143, 929-944.
14. Waqas, H., Imran, M., Khan, S. U., Shehzad, S. A., & Meraj, M. A. (2019). Slip flow of Maxwell viscoelasticity-based micropolar nanoparticles with porous medium: a numerical study. Applied Mathematics and Mechanics, 40, 1255-1268.
15. Khan, S. U., Tlili, I., Waqas, H., & Imran, M. (2021). Effects of nonlinear thermal radiation and activation energy on modified second-grade nanofluid with Cattaneo–Christov expressions. Journal of Thermal Analysis and Calorimetry, 143, 1175-1186.
16. Song, Y. Q., Khan, S. A., Imran, M., Waqas, H., Khan, S. U., Khan, M. I., ... & Chu, Y. M. (2021). Applications of modified Darcy law and nonlinear thermal radiation in bioconvection flow of micropolar nanofluid over an off centered rotating disk. Alexandria Engineering Journal, 60(5), 4607-4618.
17. Siddiqui, B. K., Batool, S., Malik, M. Y., ul Hassan, Q. M., & Alqahtani, A. S. (2021). Darcy Forchheimer bioconvection flow of Casson nanofluid due to a rotating and stretching disk together with thermal radiation and entropy generation. Case Studies in Thermal Engineering, 27, 101201.
18. Khan, U., Bilal, S., Zaib, A., Makinde, O. D., & Wakif, A. (2022). Numerical simulation of a nonlinear coupled differential system describing a convective flow of Casson gold–blood nanofluid through a stretched rotating rigid disk in the presence of Lorentz forces and nonlinear thermal radiation. Numerical Methods for Partial Differential Equations, 38(3), 308-328.

19. Shaheen, N., Ramzan, M., & Alaoui, M. K. (2021). Impact of Hall current on a 3D Casson nanofluid flow past a rotating deformable disk with variable characteristics. Arabian Journal for Science and Engineering, 46(12), 12653-12666.

20. Jyothi, A. M., Naveen Kumar, R., Punith Gowda, R. J., Veeranna, Y., & Prasannakumara, B. C. (2021). Impact of activation energy and gyrotactic microorganisms on flow of Casson hybrid nanofluid over a rotating moving disk. Heat Transfer, 50(6), 5380-5399.

21. Yu, B., Ramzan, M., Riasat, S., Kadry, S., Chu, Y. M., & Malik, M. Y. (2021). Impact of autocatalytic chemical reaction in an Ostwald-de-Waele nanofluid flow past a rotating disk with heterogeneous catalysis. Scientific Reports, 11(1), 15526.

22. Hayat, T., Khan, M. W. A., Khan, M. I., Waqas, M., & Alsaedi, A. (2018). Impact of chemical reaction in fully developed radiated mixed convective flow between two rotating disk. Physica B: Condensed Matter, 538, 138-149.

23. Mehmood, T., Ramzan, M., Howari, F., Kadry, S., & Chu, Y. M. (2021). Application of response surface methodology on the nanofluid flow over a rotating disk with autocatalytic chemical reaction and entropy generation optimization. Scientific Reports, 11(1), 4021.

24. Song, Y. Q., Khan, S. A., Imran, M., Waqas, H., Khan, S. U., Khan, M. I., ... & Chu, Y. M. (2021). Applications of modified Darcy law and nonlinear thermal radiation in bioconvection flow of micropolar nanofluid over an off centered rotating disk. Alexandria Engineering Journal, 60(5), 4607-4618.

25. Khan, M. I., Waqas, H., Khan, S. U., Imran, M., Chu, Y. M., Abbasi, A., & Kadry, S. (2021). Slip flow of micropolar nanofluid over a porous rotating disk with motile microorganisms, nonlinear thermal radiation and activation energy. International Communications in Heat and Mass Transfer, 122, 105161.